JOURNAL OF CATALYSIS 147, 552–566 (1994)

A TAP Reactor Investigation of C_6 Reforming on Nonacidic and Acidic Supported Metal Catalysts

David S. Lafyatis, Gilbert F. Froment,[1] Anne Pasau-Claerbout, and Eric G. Derouane

Laboratorium voor Petrochemische Techniek, Universiteit Gent, Krijgslaan 281, B-9000 Gent, Belgium; and Département de Chimie-Laboratoire de Catalyse, Facultés Universitaires Notre-Dame de la Paix, 61 Rue de Bruxelles, B-5000 Namur, Belgium

Received September 15, 1993; revised January 27, 1994

The reforming of C_6 hydrocarbons on Pt/Mg(Al)O, Pt/K–L, Pd/Mg(Al)O, and Pt–Re/Al_2O_3 (sulfided and unsulfided forms) has been investigated using the temporal analysis of products (TAP) reactor. Pulse experiments with several different pure C_6 feeds were performed in a continuous flow of H_2 at a pressure of 1 bar and temperatures between 400 and 510°C. Under these conditions the reaction network for all of the catalysts appeared to occur by a monofunctional metal pathway: methylpentane → methylcyclopentane → *n*-hexane → benzene. Evidence of partially dehydrogenated linear C_6 molecules as intermediates between *n*-hexane and benzene was also obtained. Turnover frequencies and benzene selectivities for the Pt/Mg(Al)O and the Pt/KL catalysts were comparable. For the Pd/Mg(Al)O catalyst the selectivity to benzene was higher and the turnover frequency was lower. Because the TAP technique reflects only the activity of truly active catalytic sites, the turnover frequencies from this study (10–12 sec^{-1} at 425°C on Pt) are higher than generally reported in the literature. Previous investigations of the Pt–Re/Al_2O_3 catalyst under industrial conditions have shown that the bifunctional mechanism was dominant. The monofunctional mechanism found here implies the existence of two dehydrocyclization pathways on these catalysts: a monofunctional metal pathway favored at low pressures, and a bifunctional pathway which is dominant at higher pressures. © 1994 Academic Press, Inc.

INTRODUCTION

The reforming of naphtha is generally carried out on Pt/Al_2O_3 and Pt–Re/Al_2O_3 catalysts. Under industrial conditions these catalysts are dual functional, hydrogenation/dehydrogenation reactions occurring on the metallic sites, and isomerization and dehydrocyclization reactions occurring on the acidic sites of the Al_2O_3 support (1). The balancing of these two reaction steps is crucial to the performance of the catalyst. Also critical to the optimization of the reforming process is the suppression of hydrogenolysis on the metal sites. To limit the activity of the metal sites for hydrogenolysis, it is general practice to presulfide the Pt/Al_2O_3 and Pt–Re/Al_2O_3 catalysts. Although there has been much speculation regarding the precise interactions of the sulfur species with the metallic sites, the improved performance of the Pt and Pt–Re catalysts due to presulfiding has been clearly demonstrated (2–4).

It has been known for many years that Pt supported on nonacidic carriers also catalyzes dehydrocyclization reactions (5–7). In the past decade, a new generation of reforming catalysts consisting of Pt supported on nonacidic materials has been investigated. Pt/KL (Pt supported on potassium exchanged Na–L zeolite) was shown to have excellent selectivity for the conversion of *n*-hexane to benzene (8, 9). This has been attributed to structural effects of the zeolite leading to preferential ring closure of *n*-hexane by the 1/6 instead of the 1/5 pathway (9–11). This is followed by the rapid dehydrogenation of the six-membered ring to benzene, rather than the more varied reactions which occur from methylcyclopentane. The Pt/KL catalyst is highly susceptible to poisoning by sulfur and thus requires feeds of extremely high purity (12).

Recently, Davis and Derouane (13, 14) have shown that Pt supported on a nonmicroporous, nonacidic carrier Mg(Al)O also selectively converts hexane into benzene. The Mg(Al)O support is a stabilized magnesium oxide, prepared by the coprecipitation of magnesium nitrate and aluminum nitrate, which retains a high surface area (200 m^2/g) after high temperature calcination (15). The benzene selectivity of this catalyst clearly does not rely upon steric effects from the support. Possible explanations included unidentified metal–support interactions, a bifunctional basic/metal mechanism, or improved dispersion of the metal. Further work showed that Pd supported on Mg(Al)O leads to an even higher selectivity for *n*-hexane dehydrocyclization (16), although the activity of this catalyst was somewhat lower than that of Pt/Mg(Al)O (17).

In the present paper, the temporal analysis of products (TAP) reactor has been used to investigate the mechanism of reforming on Pt/Mg(Al)O, Pd/Mg(Al)O, Pt/KL, and an industrial Pt-Re/Al_2O_3 catalyst, which was considered

[1] To whom correspondence should be addressed.

0021-9517/94 $6.00

in both the unsulfided and presulfided forms. The rate of benzene production from a variety of C_6 feeds was examined. The unique properties of the TAP reactor allowed important mechanistic conclusions to be drawn for each catalyst.

EXPERIMENTAL

Catalysts

Five different catalysts have been investigated; Pt/Mg(Al)O, Pd/Mg(Al)O, Pt/KL (Pt supported on potassium exchanged zeolite L), Pt-Re/Al_2O_3, and Pt–Re–S/Al_2O_3 (sulfided Pt-Re/Al_2O_3). The preparation of the Pt/Mg(Al)O (0.9% Pt), Pd/Mg(Al)O (1.0% Pd), and Pt/KL (0.5% Pt) catalysts has been previously described (13, 14, 16). The samples used in the TAP experiments came directly from a batch which had been investigated in steady-state reactor experiments. Thus, the only pretreatment that these catalysts received was *in situ* reduction in hydrogen flow (1 atm) at 477°C for several hours. The fraction of metal atoms exposed after reduction at 477°C has been estimated previously for the two Pt catalysts by H_2 chemisorption. Pt/KL had a dispersion of 1.0 and Pt/Mg(Al)O had a dispersion of 0.49 (13, 14), meaning that the total number of Pt atoms exposed per gram of catalyst was nearly the same.

The industrial Pt–Re/Al_2O_3 catalyst (CK-433 from Akzo, 0.3% Pt, 0.3% Re) has previously been characterized thoroughly in this laboratory (4, 18, 19). In the case of the unsulfided catalyst, calcination and reduction at 510°C were performed *in situ* in the TAP reactor. Two different samples of presulfided catalyst were examined. A freshly presulfided catalyst (Pt–Re–S/Al_2O_3-fresh) was calcined, reduced, and sulfided in a separate unit to prevent the contamination of the TAP system with sulfur. The sulfiding was done as previously described using a 1% H_2S in hydrogen mixture (20), after which weakly bound sulfur was stripped from the catalyst in H_2 flow at 500°C. The catalyst was then cooled to ambient temperature under hydrogen flow prior to removal from the presulfiding unit. In addition, a Pt–Re–S/Al_2O_3-aged catalyst sample which had been used previously in reforming experiments (20) was tested. The presence of sulfur was confirmed on both of the sulfided catalysts by energy dispersive X-ray (EDX) analysis. The freshly presulfided catalyst and the aged catalyst were both reduced at 510°C in H_2 flow after being placed into the TAP system.

TAP Reactor System

A schematic diagram of the TAP system is shown in Fig. 1. Detailed descriptions of the TAP apparatus are available elsewhere (21), and thus only a brief discussion will be given here to emphasize the key features of the

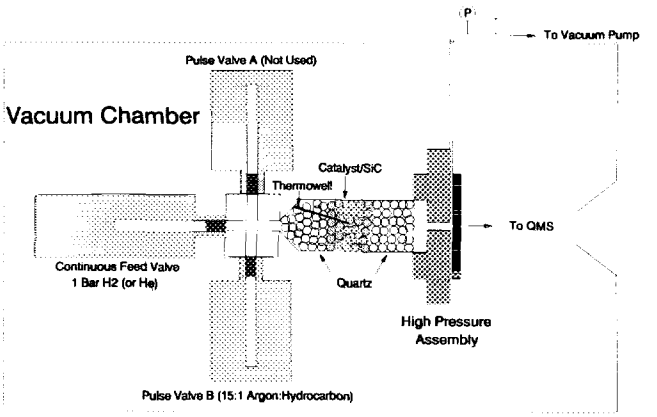

FIG. 1. TAP reactor system used for reforming experiments.

unit pertinent to this investigation. The elevated-pressure assembly described previously (22) was utilized throughout the study to allow a constant pressure of approximately 1 bar in the reactor. In most experiments this pressure was maintained by a flow of hydrogen (99.99%) at a constant rate of approximately 0.25 NL/min. Some experiments were performed using a helium flow (99.996%) instead of hydrogen. The microreactor was approximately 40 mm long with an inner diameter of 6 mm. The packing of the microreactor consisted of a 12-mm inlet section of quartz beads, a 9-mm section of the active catalyst phase diluted by SiC, and a 10-mm outlet section of quartz beads. The particle size was 0.25–0.50 mm for all materials. The amount of catalyst utilized in the reactor bed was varied according to the reactivity of each catalyst. The use of the high-pressure assembly precluded measuring the reactor temperature directly inside the catalyst bed. Thus, the original microreactor was redesigned to allow the temperature to be measured and controlled using a single thermocouple inserted in a narrow well which protruded at an angle into the reactor.

Pulses of an argon/hydrocarbon mixture (approximately 15 : 1) were introduced directly to the inlet of the reactor from a zero-dead-volume manifold. The pulse valves emit extremely small and narrow pulses (approximately 10^{16} molecules per pulse), guaranteeing that only a small portion of the available catalyst sites were utilized during any given pulse. Thus, the kinetics of individual sites could be studied under conditions of low hydrocarbon coverage. Because of the continuous hydrogen carrier flow, the ratio of H_2/hydrocarbon under normal experimental conditions was extremely high.

When using the high-pressure assembly, the outlet flow from the TAP microreactor is split into two streams. Most of the effluent flow is directed through a metering valve which is backed by a mechanical pump. By adjusting the pressure at the inlet of the reactor and the metering valve at the outlet of the reactor, the pressure and the flow rate

in the reactor may be controlled. A small portion of the reactor effluent is directed through a 0.001-inch pinhole leak (heated to 80°C, the upper limit suggested by the manufacturer) and then immediately towards a quadrupole mass spectrometer (QMS) for analysis. The time required for transport to the mass spectrometer is negligible compared to other effects in the reactor. Thus, the signal transmitted to the QMS ideally reflects only the transport and adsorption/reaction/desorption occurring within the reactor. The QMS may be tuned to observe the mass of a significant peak in the mass spectrum for the molecule of interest. The spectrometer monitors the desired mass at a rate of 10,000 times per second, permitting excellent resolution of the response curve at that mass. The signal-to-noise ratio is further enhanced by averaging the signal over 50–100 pulses. Duplicate experiments performed while monitoring different masses allow the detection of a variety of different reaction products.

One complication in the study of reforming using the QMS detector of the TAP reactor is the overlapping mass signals of many important product molecules. Argon (the internal standard) and benzene were monitored satisfactorily at $m/e = 40$ and $m/e = 78$, respectively. Other components such as *n*-hexane, methylpentanes, dimethylbutanes, hexenes, methylpentenes, cyclohexane, and methylclopentane do not have unique mass signals which could be monitored for identification. Thus it is not possible for the QMS to measure a unique mass signal for each of the components produced in reforming. A compromise solution is to treat the system by lumping certain similar species and then deconvoluting the response curves for these pseudocomponents from the measured mass response curves. The complete development of the equations used in this study for the deconvolution of the C_6 component peaks from the mass response peaks is presented in the Appendix. For components smaller than C_6 the deconvolution of the mass peaks becomes intractable, and thus no attempt was made to identify products of hydrogenolysis or hydrocracking in this study.

Response curves for the major C_6 components from pulsing several different pure-component hydrocarbon feeds over each type of catalyst were examined. An additional tool for examining the reaction network for a given catalyst is to compare the benzene response curves which resulted from different feeds under identical reactor conditions. This requires that the carrier gas flow rate and the catalyst properties remain constant during the complete set of experiments. The argon peak was used to monitor the carrier flow rate during each set of experiments. The consistent shape and position of this inert peak guaranteed that the carrier gas flow rate remained constant. In order to ensure that the catalyst's behavior remained steady, an entire set of feeds was tested during a single day, and the reproducibility of the benzene curve from the first hydrocarbon examined (generally 2-methylpentane) was checked at the end of the day.

Several feeds were investigated over the various catalysts, including benzene, cyclohexene, cyclohexane, 1,5-hexadiene, 1-hexene, 2-hexene, *n*-hexane, methylcyclopentane, 2-methylpentane, and 3-methylpentane. The Pt/Mg(Al)O, Pd/Mg(Al)O, and Pt/KL catalysts were investigated at temperatures between 400 and 477°C. The Pt–Re/Al_2O_3 catalysts were investigated at 477 and 510°C, because slow benzene desorption from the catalyst resulted in response curves which did not return to the baseline in a reasonable time interval at lower temperatures. For all catalysts, each feed was also tested at 250°C. At this temperature no reaction occurred for several of the feeds, including methylpentane, methylcyclopentane, *n*-hexane, and cyclohexane. The olefins and di-olefins underwent rapid hydrogenation at 250°C.

RESULTS AND DISCUSSION

Control Experiments

A series of control experiments were performed to characterize the transport of the various feed molecules through an inert (glass) reactor bed under typical reactor conditions (H_2 flow = 0.25 NL/min), pressure = 1 bar, temperature = 477°C). Figure 2 shows the normalized transient responses of argon, 2-methylpentane, *n*-hexane, methylcyclopentane, cyclohexane, and benzene pulses over a bed of pure SiC in the reactor section. The small differences in elution shown in Fig. 2 were caused by condensation of the hydrocarbons in the pinhole leak described previously. This delayed elution of the relatively heavy hydrocarbon molecules used in this study was unavoidable, due to the prescribed temperature limit of the

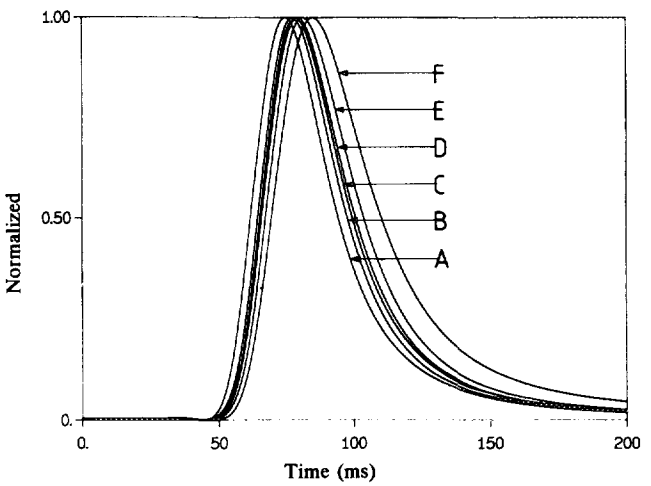

FIG. 2. Normalized feed responses, inert bed, 477°C, H_2 flow. (A) Argon; (B) 2-methylpentane; (C) *n*-hexane; (D) methylcyclopentane; (E) cyclohexane; (F) benzene.

pinhole leak, and was found to be quite reproducible. Beyond this exit effect, the transport through the bed of all the hydrocarbons was quite similar, as shown by the similar shapes of the response curves.

Control experiments under typical reaction conditions with an inert reactor bed indicated that most of the feed components did not react in the absence of catalyst. The exceptions were cyclohexene dehydrogenation to benzene (about 15% conversion of a cyclohexene pulse at 477°C), and trace amounts of hexadiene and hexene hydrogenation.

Separate control experiments were also performed with bare Mg(Al)O, KL, and Al_2O_3 supports in the reactor bed. No reaction of hydrocarbon feeds on any of the supports was evident at temperatures between 250 and 510°C. At 250°C Mg(Al)O interacted with pure feeds of hexadiene, hexene, and benzene, resulting in elution curves which were significantly delayed and more spread out than the elution curves from saturated hydrocarbon feeds. However, at the higher temperatures used during the reforming studies (400–477°C), the presence of the Mg(Al)O support had virtually no effect on the response curves of any of the hydrocarbon feeds relative to an inert bed. This indicated that under reforming conditions, adsorption and intraparticle transport in the Mg(Al)O support did not affect the hydrocarbon response curves. Similarly, on the zeolite KL support at 250°C the response curves for all of the hydrocarbon feeds were considerably delayed compared to the inert. Above 400°C, however, the response curves of the hydrocarbons were nearly unaffected by the presence of the support. Thus, intraparticle transport and adsorption in the zeolite KL support did not have a significant effect on the shape and position of the hydrocarbon response curves at reforming temperatures. Minor adsorption interactions of the unsaturated hydrocarbons on the Al_2O_3 support were observed at all temperatures.

Reaction Mechanism

Pt/Mg(Al)O. Previous experimental investigations of Pt/Mg(Al)O, Pt/KL, and Pd/Mg(Al)O by Derouane and co-workers (13, 14, 16) were performed at 1 atm and 6 : 1 H_2/hydrocarbon ratio. The conditions employed in the present TAP study are similar, except that hydrocarbon is present in much lower concentrations.

Figures 3a–3c illustrate the transient responses from a pulse experiment with a *n*-hexane feed over the Pt/Mg(Al)O catalyst at 477°C with H_2 flow. Figure 3a displays the normalized QMS response curves at m/e = 40, 69, 71, 78, 84, and 86. As discussed previously, the curve at m/e = 40 (curve A) is the argon internal standard, and the curve at m/e = 78 (curve F) is the benzene response curve. The four remaining curves are all combinations of multiple components. In Fig. 3b, the peak deconvolution method has been applied to the mass response curves. This plot has been normalized, and provides a useful picture of reaction products starting from a *n*-hexane feed. Argon elutes first, followed by *n*-hexane (curve B). Curve C is the curve which theoretically represents the lump of normal hexenes, branched hexenes, and cyclohexane. Because this lump elutes rapidly after *n*-hexane, curve C likely represents almost entirely normal hexenes. Response curves D and E are the curves for methylcyclopentane and the methylpentanes, respectively. These curves lie almost directly on top of each other, but in lower temperature experiments it was clear that the methylcyclopentane curve preceded the methylpentane curve. The final component to appear is benzene. The tail of benzene extending beyond the tail of all the other products is a feature seen throughout the reforming experiments, and arises because benzene is the final component in a reaction network of reversible reactions. Thus, because benzene may be formed from each of the other C_6 compounds, it continues to elute until all other components have left the reactor or have been consumed.

Figure 3c has not been normalized, and thus gives a representation of the actual amount of each product formed. Curve A is the hexane feed peak. Because the conversion of *n*-hexane is quite low, this peak is extremely large, and thus the top of the peak has not been shown (in Fig. 3c the top of this curve would have a relative molar concentration of 19). Curves B–E show hexene, methylcyclopentane, methylpentane, and benzene, respectively. The high selectivity of this catalyst toward benzene relative to the other C_6 compounds is clear.

The control experiments over the bare Mg(Al)O support indicated that intraparticle transport and adsorption on the support had no effect on the TAP response curves for the hydrocarbon components. Thus, the TAP response curves reflect only the effects of convective gas-phase transport and adsorption/reaction/desorption on the metal site. An interesting method of investigating the reforming reaction network was to compare the benzene response curves from several different hydrocarbon feeds under identical reactor conditions. Figures 4a and 4b show a series of benzene response curves from the Pt/Mg(Al)O catalyst at 425 and 477°C, respectively. Because the carrier flow rate was kept constant, convective gas-phase transport in the reactor should not affect the comparison of these curves. Also, because benzene is always the product under observation, the minor condensation at the reactor exit should have an identical effect on each curve. Thus, only the phenomena of adsorption, reaction, and desorption are left in the comparison of these benzene response peaks. Experiments at 250°C (at which temperature only hydrogenation reactions occurred) indicated that, except in the case of benzene, the response curves for the hydrocarbon feeds were not significantly affected

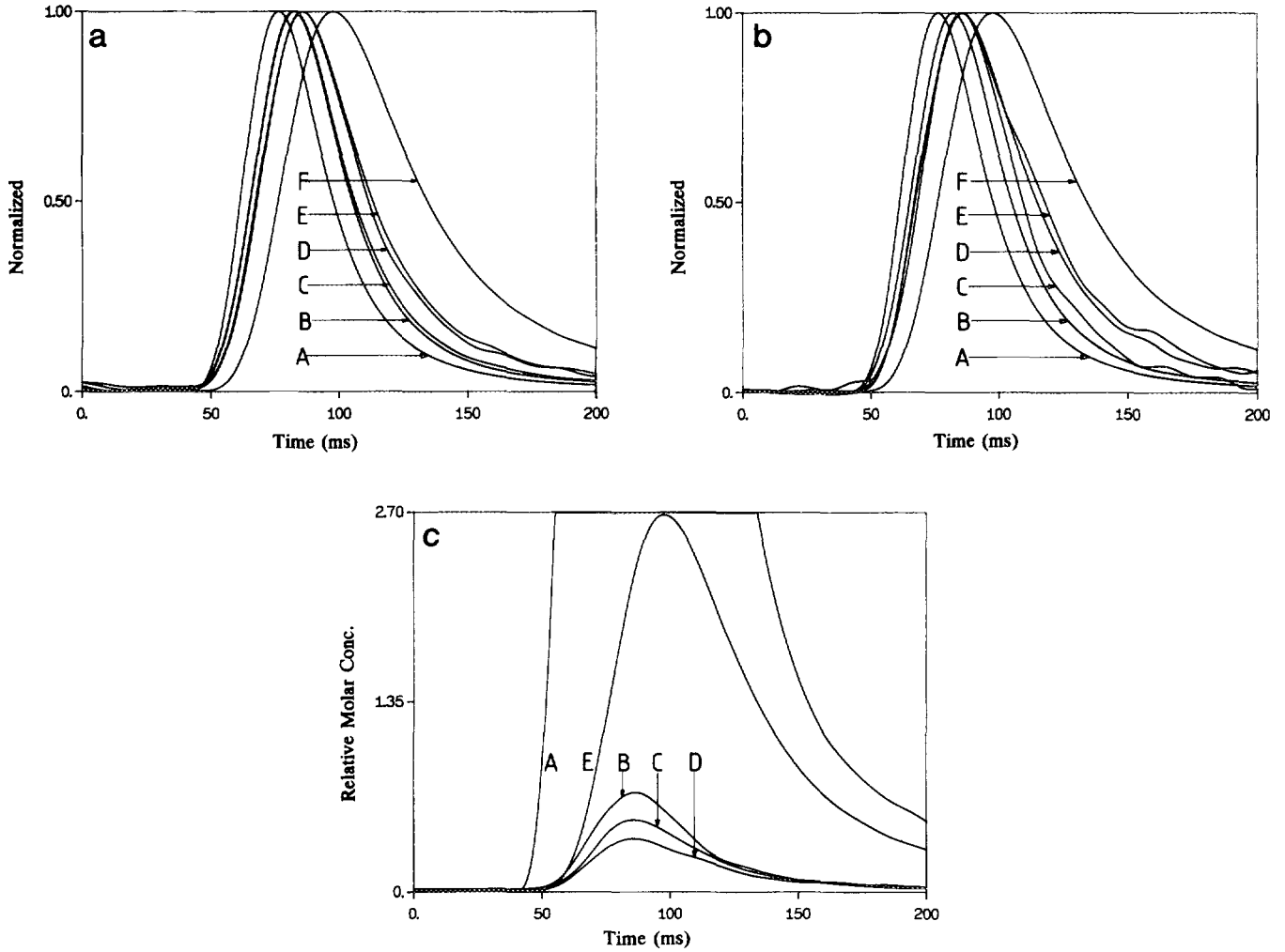

FIG. 3a. Normalized *m/e* response curves, *n*-hexane feed: Pt/Mg(Al)O Catalyst Bed, 477°C, H_2 flow. (A) *m/e* = 40; (B) *m/e* = 86; (C) *m/e* = 71; (D) *m/e* = 84; (E) *m/e* = 69; (F) *m/e* = 78.

FIG. 3b. Normalized product response curves, *n*-hexane feed: Pt/Mg(Al)O, 477°C, H_2 flow. (A) Argon; (B) *n*-hexane; (C) hexene; (D) methylcyclopentane; (E) methylpentane; (F) benzene.

FIG. 3c. Product response curves, *n*-hexane feed: Pt/Mg(Al)O, 477°C, H_2 flow. (A) *n*-Hexane; (B) hexene; (C) methylcyclopentane; (D) methylpentane; (E) benzene.

by the presence of the catalyst. This suggests that adsorption and desorption of reactants and intermediate products were not significantly slow steps in the dehydrocyclization reaction, and thus had little bearing on the benzene response curves.

The remaining factors to consider in Figs. 4a and 4b are the reaction time for the given hydrocarbon to form benzene, the desorption time for benzene from the catalyst surface, and possible readsorption/desorption time of benzene further down the bed. The desorption rate of benzene from the catalyst surface after formation should not depend on the original hydrocarbon reactant, and so it poses no difficulty for the comparison of benzene response curves from different hydrocarbons. The effects of readsorption of benzene on other sites in the bed could be problematic, however, because molecules produced from reactants closer to benzene in the reaction network may be produced (on average) earlier in the bed, and thus have a greater chance for readsorption. In order to minimize this effect, two precautions were taken throughout the experiments:

1. Conversion of the feed hydrocarbons was kept at low to moderate levels.

2. Benzene response curves from a benzene feed were measured for each catalyst.

The first precaution should result in benzene response curves least affected by benzene readsorption in the bed. The measurement of a benzene response curve resulting from a benzene feed provides the limiting case of the maximum possible benzene readsorption/desorption in

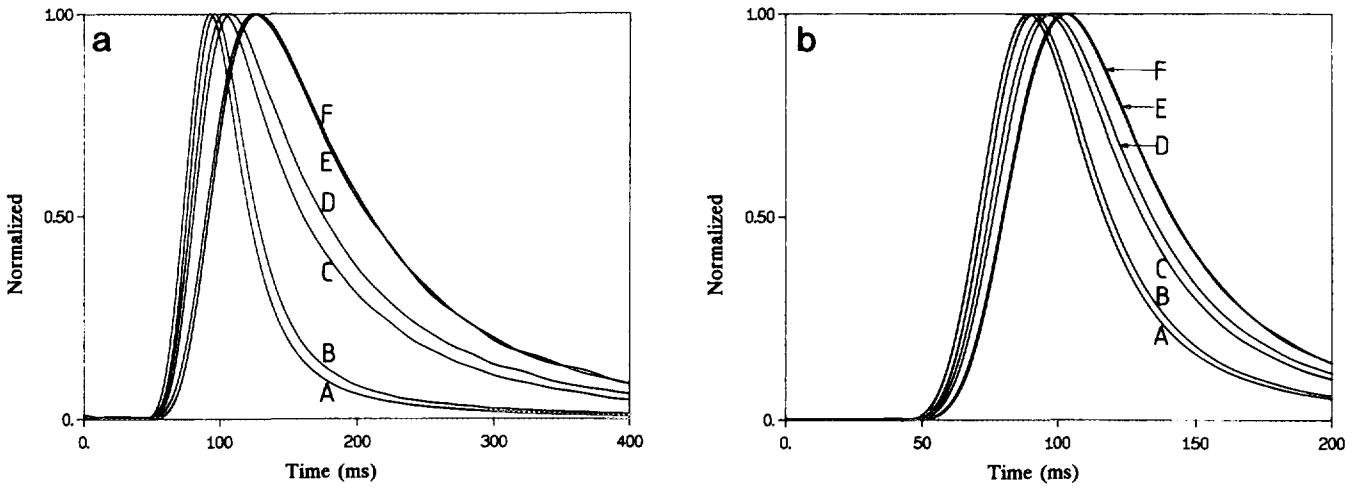

FIG. 4. Normalized benzene response curves: (a) Pt/Mg(Al)O, 425°C, H_2 flow; (b) Pt/Mg(Al)O, 477°C, H_2 flow. (A) Benzene feed, cyclohexene feed; (B) cyclohexane feed; (C) 1-hexene feed, 2-hexene feed, 1,5-hexadiene feed; (D) *n*-hexane feed; (E) methylcyclopentane feed; (F) 2-methylpentane feed, 3-methylpentane feed.

the catalyst bed. If benzene desorption were the rate-determining step, the benzene response curve from a benzene feed would appear later than the benzene curve produced from hydrocarbon feeds because the benzene produced from the hydrocarbon feed would have less chance for re-adsorption. Consistently throughout the study the benzene response curves from the benzene pulses gave the most rapid responses, indicating that the surface reactions played the dominant role in determining the relative positions of the curves.

Following the above discussion, Figs. 4a and 4b give a rather complete view of the reaction sequence of C_6 hydrocarbons on Pt/Mg(Al)O. These figures display the normalized curves for benzene at 425 and 477°C in H_2 flow from several different hydrocarbon feeds. Curve A in Fig. 4a shows the benzene response from a feed of benzene. This is the limiting case in which no reaction occurs, and only adsorption and desorption of benzene is present. A feed of pure cyclohexene to the reactor resulted in virtually complete conversion to benzene and yielded a benzene response curve which fell identically on top of curve A. This indicates that the conversion from cyclohexene to benzene is extremely rapid. Curve B shows the benzene response from the cyclohexane feed. This curve is shifted to a later elution time than curve A, thus indicating that the conversion from cyclohexane to benzene is significantly slower than that from cyclohexene to benzene. This implies that the first dehydrogenation of the cyclohexane molecule is the slow step, followed by rapid dehydrogenation of the remaining olefinic ring species. The cyclohexane feed generally did not undergo significant reverse reactions, as is evident from the lack of ring-opening products in the effluent. Curve C is the benzene response from a 1-hexene feed. This response curve appears significantly later than the response curves from the ringed-component feeds, indicating that 1,6 closure of the ring is rather slow. Separate experiments with a 2-hexene feed and with a 1,5-hexadiene feed gave response curves identical to curve C, implying that the interconversion between these partially dehydrogenated C_6 species is rapid, or that the dehydrocyclization reaction proceeds at the same rate from each of these feeds. Curve D shows the benzene response from the *n*-hexane feed. This curve is shifted to a later time than the curve from the olefinic C_6 species. Curves E and F show the benzene response curves from methylcyclopentane and 2-methylpentane, respectively. These curves are very close to each other, with the benzene response curve of methylcyclopentane slightly preceding that of 2-methylpentane. 3-Methylpentane was also fed to the reactor and gave a benzene response identical to that of the 2-methylpentane feed.

Figure 4b shows the benzene responses from the same feeds as Fig. 4a, but at 477°C. All of the benzene response curves now elute more rapidly from the reactor, indicating faster reaction rates due to the increase in temperature. The elution order remains the same as in Fig. 4a, although at this higher temperature curves E and F are nearly indistinguishable.

Figure 5 shows the resulting benzene response curves when the three linear C_6 hydrocarbons are fed to the catalyst at 477°C under He flow, instead of H_2. In the absence of hydrogen the elution curves of 1,5 hexadiene and 1-hexene were separated from each other, with the 1,5-hexadiene feed clearly producing benzene more rapidly than 1-hexene. Under the H_2 flow conditions given in Figs. 4a and 4b, the hexadiene was probably hydrogenated rapidly to hexene before ring closure could occur. In the

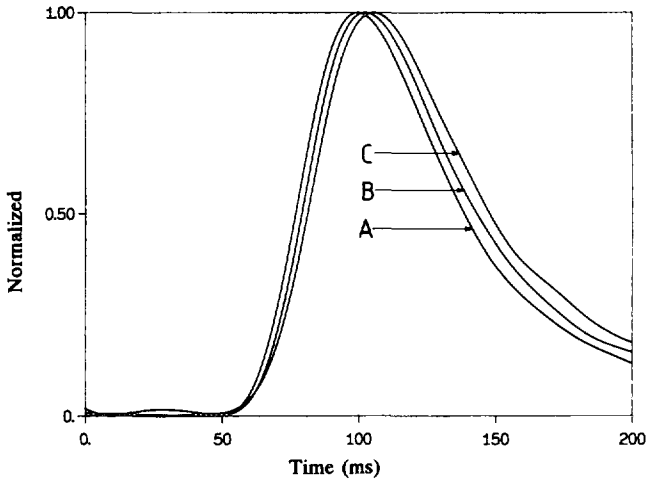

FIG. 5. Normalized benzene response curves: Pt/Mg(Al)O, 477°C, He flow. (A) 1,5-Hexadiene feed; (B) 1-hexene feed; (C) *n*-hexane feed.

absence of hydrogen flow this hydrogenation could not occur, thus allowing the more dehydrogenated feed to produce benzene more rapidly than the less dehydrogenated feed.

The curves presented in Figs. 3–5 provide a straightforward picture of the reaction pathway for C_6 hydrocarbon conversion to benzene over the Pt/Mg(Al)O catalyst. Figure 6 shows this reaction network. As shown in Figs. 4a and 4b methylpentane requires the longest time to produce benzene. Thus, this component is shown as the first component in the reaction network. Methylpentane undergoes 1,5 ring closure, as was confirmed by the rapid production of methylcyclopentane from a 2-methylpentane feed. The clear similarity between curves E and F suggests that these two reactants are closely related to each other. It does not appear that direct isomerization of methylpentane to *n*-hexane without passing through a C_5 ring intermediate occurs to any significant extent. This is in agreement with previous work on well-dispersed supported Pt catalysts (23–25).

Methylcyclopentane undergoes ring opening to form methylpentane (the reverse of the reaction discussed in the previous paragraph) and *n*-hexane. Direct ring expansion of methylcyclopentane to a C_6 ring does not seem to occur, as indicated by the intermediate production of *n*-hexane from methylcyclopentane, and the more rapid formation of benzene from *n*-hexane than from methylcyclopentane. The similarity between opening of a naphthenic ring and paraffin hydrogenolysis (which passes through dehydrogenated surface intermediates (1)) implies that the linear C_6 surface species formed from methylcyclopentane may be unsaturated. Under reducing conditions, this surface species is expected to form *n*-hexane, and the mechanism in Fig. 6 shows the direct conversion from methylcyclopentane to *n*-hexane. However, this dehydrogenated surface species may also lead to benzene without becoming saturated. The mechanism on the Pt/Mg(Al)O catalyst, at the conditions employed in this study, is clearly different from the well-established bifunctional mechanism in which methylcyclopentane is an intermediate species in *n*-hexane dehydrocyclization. The dehydrocyclization mechanism in which methylcyclopentane passes through a linear C_6 intermediate during conversion to benzene has been previously proposed for Pt supported on nonacidic Al_2O_3 (6) and Pt/KL (9) catalysts, and is considered a monofunctional reaction network on the metal.

n-Hexane is apparently dehydrogenated at least once to hexene prior to 1,6 ring closure. This is supported by three observations:

1. Hexene rapidly appears from the *n*-hexane feed (Fig. 3b, curve C).

2. Hexene produces benzene more rapidly than *n*-hexane, as shown in Fig. 4.

3. Previous steady-state reactor studies of this catalyst showed a large amount of hexene in the effluent (13, 14). Further dehydrogenation of hexene to hexadiene as an intermediate species before ring closure is also likely. This second dehydrogenation step would be expected to take place more easily than the paraffin dehydrogenation, and in the experiments performed in the absence of hydrogen, benzene was formed more rapidly from hexadiene than from hexene. Interference from other peaks made it impossible to positively identify hexadienes as intermediates during the pulse experiments. Further dehydrogena-

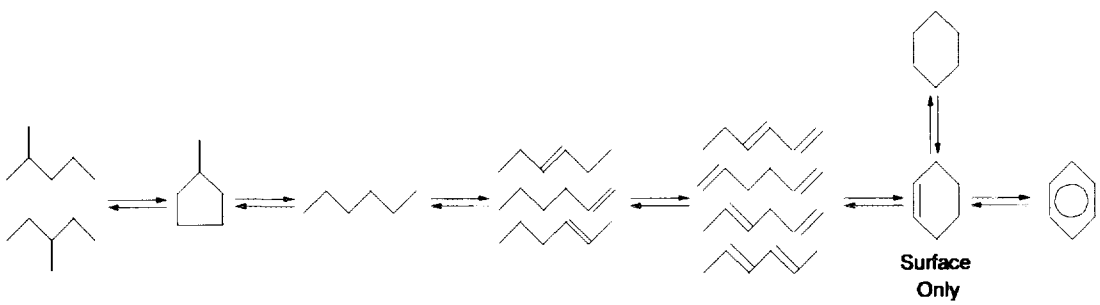

FIG. 6. Proposed network of C_6 reforming reactions for Pt/Mg(Al)O, Pt/KL, and Pd/Mg(Al)O.

tion of the linear C_6 species to hexatriene prior to ring closure also cannot be ruled out.

Which species is formed upon 1,6 ring closure of the partially dehydrogenated C_6 species is not certain. It appears unlikely, however, that cyclohexane is an intermediate in the dehydrocyclization reaction network. If hexadiene (or hexatriene) is the linear C_6 intermediate prior to 1,6 cyclization, formation of the saturated cyclohexane ring upon ring closure would be unexpected. In addition, cyclohexane is generally not found in significant quantities in the effluent of hexane reforming studies. As shown by Figs. 4a and 4b the reaction time for cyclohexane dehydrogenation to benzene is significant, suggesting that if the naphthenic ring were formed it should be able to desorb and appear in the product stream. The partially dehydrogenated ring species evidently react much more rapidly to benzene. This accounts for their absence in the effluent of reactor studies, and implies that they exist only as surface species in the reforming reaction mechanism.

The benzene response curves in Figs. 4a and 4b may be divided into three groups, according to the feeds: C_6 ring compounds (benzene, cyclohexene, and cyclohexane), C_6 linear components (*n*-hexane, hexenes, and hexadiene), and substituted C_5 compounds (methylpentanes and methylcyclopentane). The two significant steps in the reaction sequence (Fig. 6) involve transformations from one group to another: the opening of the methyl-substituted C_5 ring to a linear C_6 molecule and the ring closure of the linear C_6 molecule.

On the Pt/Mg(Al)O catalyst, 1,5 ring closure of methylpentane is much more rapid than 1,6 ring closure of *n*-hexane. The distance (time difference) between Curves F and E, the benzene response curves from the methylpentane and methylcyclopentane feeds, is much shorter than the distance between Curves C and B, the benzene response curves from the *n*-hexane and cyclohexane feeds (actually, because cyclohexane is apparently not in the reaction network, Curve A from the cyclohexene feed may be more appropriate in the comparison). This result is consistent with previous work (23) which showed that, for 3-methylhexane, 1,5 ring-closure was favored over 1,6 ring closure on a well-dispersed Pt catalyst.

Pt/KL. The results from the Pt/KL catalyst present a similar picture as those from the Pt/Mg(Al)O catalyst. Figure 7 shows the benzene response curves from a series of pure hydrocarbon feeds at 425°C for the Pt/KL catalyst under H_2 flow. Two slow steps are again evident in the network, ring opening of methylcyclopentane and ring closure of the partially dehydrogenated linear C_6 molecule. The dehydrogenation of hexane to hexene and cyclohexane to cyclohexene (and benzene) is extremely rapid on this catalyst. All of the evidence from the benzene response curves of Fig. 7 and the deconvoluted response

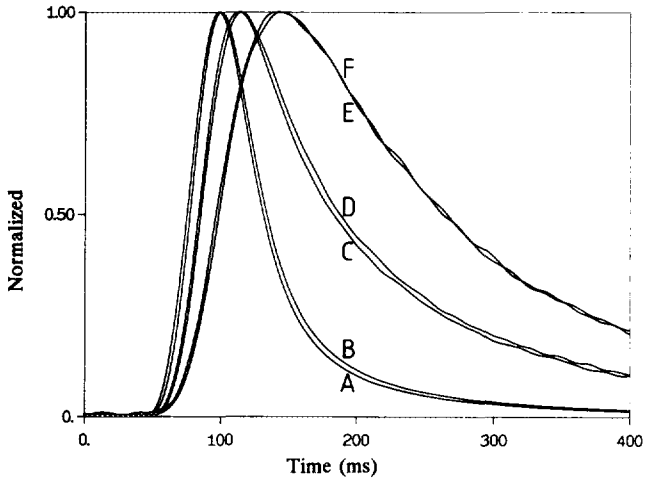

FIG. 7. Normalized benzene response curves: Pt/KL, 477°C, H_2 flow. (A) Benzene feed, cyclohexene feed; (B) cyclohexane feed; (C) 1-hexene feed, 1,5-hexadiene feed; (D) *n*-hexane feed; (E) methylcyclopentane feed; (F) 2-methylpentane feed.

curves from each feed component indicates that the reaction network on the Pt/KL catalyst is the same as that shown in Fig. 6 for the Pt/Mg(Al)O catalyst. This confirms the network for methylpentane, methylcyclopentane, hexane, and benzene that has been proposed previously for the Pt/KL catalyst (9).

Pd/Mg(Al)O catalyst. The benzene response curves from a series of pure feeds over the Pd/Mg(Al)O catalyst at 425 and 477°C are shown in Figs. 8a and 8b, respectively. The order of benzene appearance from the separate feeds is the same as discussed previously for the two Pt/Mg(Al)O and Pt/KL catalysts, implying that the reaction network is the same as that shown in Fig. 6. This was also supported by deconvolution plots of the reaction products from each feed component.

Although the order of the curves is the same as the Pt-based catalysts, there are subtle differences in the relative positions of the curves. In general, the dehydrogenation steps appear somewhat slower on the Pd/Mg(Al)O catalyst than on the Pt catalysts, as shown by the larger gaps between curves A and B (cyclohexane dehydrogenation), curves C and D (hexane dehydrogenation), and Curves E and F (methylpentane dehydrocyclization to methylcyclopentane). This is particularly clear in Fig. 8b, which shows that the classification of compounds used to describe the reaction network for the Pt-based catalysts is not accurate for the Pd catalysts. In the case of the two Pt catalysts the dehydrogenation steps were very rapid compared to the methylcyclopentane ring opening and the 1,6 ring closure reactions. For the Pd catalyst at 477°C, however, the dehydrogenation steps play a significant role in determining the overall reaction rate.

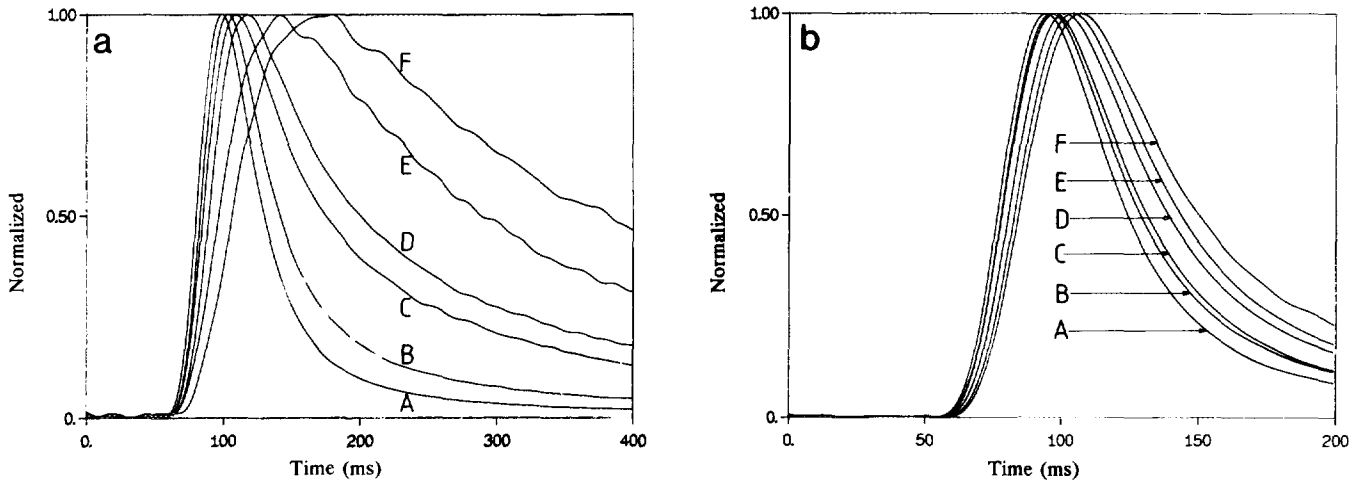

FIG. 8. Normalized benzene response curves: (a) Pd/Mg(Al)O, 425°C, H_2 flow; (b) Pd/Mg(Al)O, 477°C, H_2 flow. (A) Benzene feed, cyclohexene feed; (B) cyclohexane feed; (C) 1-hexene feed, 1,5-hexadiene feed; (D) *n*-hexane feed; (E) methylcyclopentane feed; (F) 2-methylpentane feed.

Pt–Re/Al_2O_3 and Pt–Re–S/Al_2O_3. Previous studies in this laboratory have examined bifunctional Pt/Al_2O_3 and Pt–Re/Al_2O_3 catalysts for the reforming of C_6 and C_7 hydrocarbons (3, 4, 18–20, 26). These investigations have focused on reforming under typical industrial conditions, using pressures of 4–20 bars and sulfided catalysts. Under these conditions the bifunctional mechanism was clearly established, with hydrogenation/dehydrogenation reactions occurring on the metallic sites and skeletal rearrangements occurring on the acidic sites of the carrier. Figures 9a and 9b display the acidic mechanism of skeletal carbon rearrangements for C_6 reforming on sulfided Pt/Al_2O_3 and C_7 reforming on sulfided Pt–Re/Al_2O_3 catalysts. The two mechanisms are completely analogous: direct isomerization of branched paraffins to linear paraffins, 1,5 ring closure of the linear paraffin, and ring expansion of the five-membered ring to the six-membered ring. These mechanisms reflect the preference for formation of more stabilized carbenium ions on the acidic support. Comparison of the skeletal carbon rearrangements of C_6 molecules in the monofunctional reforming and bifunctional reforming networks (Figs. 6 and 9a) shows that the crucial difference is the position of the methylcyclopentane ring in the network.

In the present work, the bimetallic bifunctional Pt–Re/Al_2O_3 catalyst was investigated in the TAP reactor. Figure 10 displays the normalized benzene response curves from the unsulfided Pt–Re/Al_2O_3 at 477°C. The order of the curves is the same as for the Pt/Mg(Al)O, Pt/KL, and Pd/Mg(Al)O catalysts discussed previously. Thus, under the conditions of the TAP experiments it appears that the monofunctional dehydrocyclization mechanism is predominant.

The positions of the benzene response curves in Fig. 10 imply that, for the metal catalyzed dehydrocyclization pathway on the Pt–Re/Al_2O_3 catalyst, the time required for dehydrogenation is rather significant. This is particularly evident when comparing curves B and C, the benzene response curves for the cyclohexane and 1-hexene feeds. The cyclohexane feed generally reacts only in the forward direction, thus only undergoing successive dehydrogenation steps (as discussed previously, only the first of these dehydrogenation steps is kinetically significant). The hexene feed has two possible directions, either forward reactions of ring closure/dehydrogenation, or the reverse direction of hydrogenation to *n*-hexane, followed by dehydrogenation and ring closure. The two choices for 1-hexene are shown clearly in Fig. 10. The leading edge of the benzene response from the 1-hexene feed lies very close to the benzene response from the cyclohexane feed. Thus, some of the hexene is never hydrogenated and undergoes cyclization (or perhaps dehydrogenation

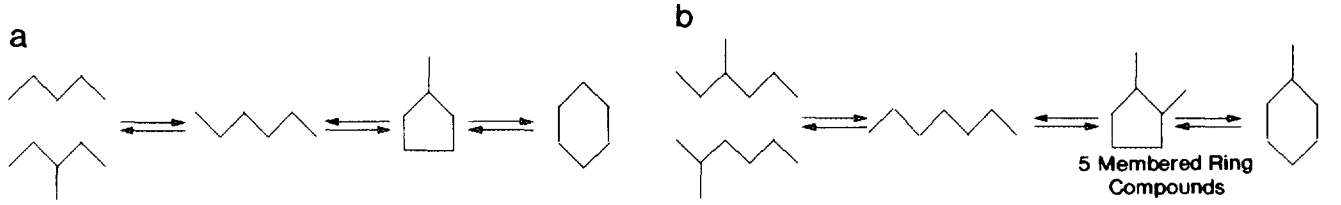

FIG. 9. Skeletal rearrangements of (a) C_6 reforming on Pt/Al_2O_3 (3) and (b) C_7 reforming on Pt–Re/Al_2O_3 (19).

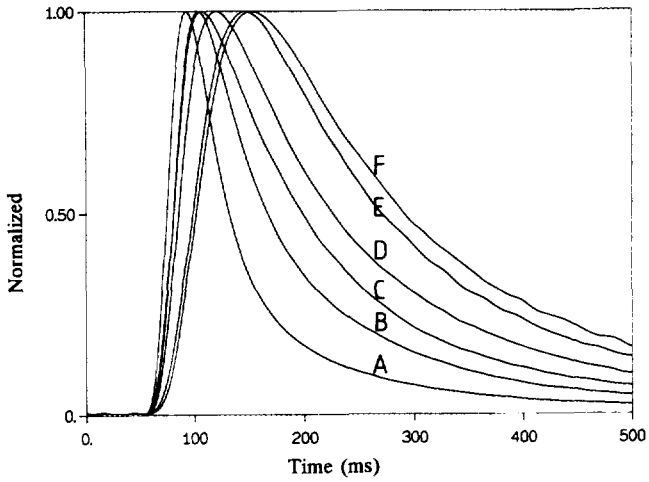

FIG. 10. Normalized benzene response curves: Pt–Re/Al_2O_3, 477°C, H_2 flow. (A) Benzene feed, cyclohexene feed; (B) cyclohexane feed; (C) 1-hexene feed; (D) *n*-hexane feed; (E) methylcyclopentane feed; (F) 2-methylpentane feed, 3-methylpentane feed.

to hexadiene, followed by cyclization), which occurs approximately as rapidly as the cyclohexane dehydrogenation reaction. Other hexene molecules are first hydrogenated to *n*-hexane, resulting in the later portion of the benzene response from 1-hexene, which more closely resembles the benzene response from the *n*-hexane feed (curve D). The similarity of the front half of the benzene curve from the linear C_6 olefin feed with the benzene curve from the naphthenic ring feed shows the significance of the dehydrogenation reaction time relative to the cyclization reaction time.

Figures 11a and 11b display an abbreviated series of benzene response curves for the Pt–Re–S/Al_2O_3-fresh and Pt–Re–S/Al_2O_3-used catalyst. In both cases the metallic dehydrocyclization network in which methylcyclopentane passes through a *n*-hexane intermediate to form benzene is still evident. Thus, under the conditions of this study, sulfiding the catalyst apparently does not significantly affect the reaction network.

Figures 10 and 11 indicate predominantely the monofunctional dehydrocyclization pathway for both the unsulfided and the sulfided Pt–Re/Al_2O_3 catalysts. This underscores the importance of operating conditions on the bifunctional reaction mechanism. The reactor conditions used for the TAP study were 1 bar H_2, with extremely small amounts of hydrocarbon in the system. The availability of metal sites under these conditions is extremely high, and the dehydrocyclization reactions are able to proceed on these sites. This is consistent with several previous studies which have indicated that, at low pressure, dehydrocyclization on bifunctional catalysts may occur by a monofunctional metal pathway (27–29). However, under industrial conditions the partial pressures of both H_2 and hydrocarbons are high, reducing the availability of metal sites due to coverage by molecular fragments. This then favors the acid catalyzed dehydrocyclization pathway previously deduced by Van Trimpont *et al.* (4, 18, 19).

Turnover Frequency and Overall Catalytic Activity

The first moment of a TAP response curve for a given component characterizes the average elution time from the reactor. Average elution time values from the reforming experiments on the Pt/Mg(Al)O, Pt/KL, and Pd/Mg(Al)O catalysts as 425°C are reported in Table 1. The first row lists the average elution time of the argon peaks. These values are nearly the same for each catalyst because the carrier flow through the reactor was approximately

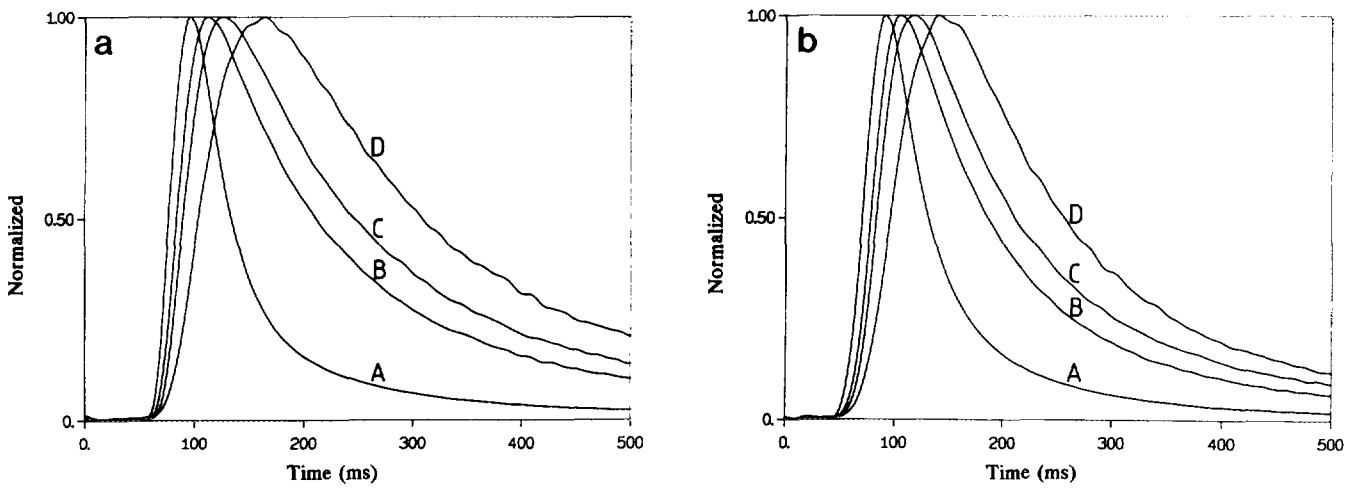

FIG. 11. Normalized benzene response curves: (a) Pt–Re–S/Al_2O_3-fresh, 477°C, H_2 flow. (A) Benzene feed, cyclohexene feed; (B) 1-hexene feed; (C) *n*-hexane feed; (D) methylcyclopentane feed. (b) Pt–Re–S/Al_2O_3-used, 477°C, H_2 flow. (A) Benzene feed; (B) 1-hexene feed; (C) *n*-hexane feed; (D) methylcyclopentane feed.

TABLE 1

Average Elution Time[a] (ms) of Response Peaks, 425°C

	Pt/Mg(Al)O	Pt/KL	Pd/Mg(Al)O
Argon	95	98	102
Benzene (inert bed)[b]	117	120	124
Benzene	123(122–125)	140(139–140)	199(180–210)
n-Hexane	205(201–211)	232(231–236)	489(471–539)
2-Methylpentane	225(219–229)	275(273–282)	627(579–676)

[a] Best estimate of average elution time is given first, followed by upper and lower bounds on the average elution time in parenthesis.

[b] Average elution time of benzene response curve from a benzene pulse in an inert bed under conditions which led to the Argon response time in the previous row.

the same for each experiment. The second row is simply the first row plus 22 ms, which accounts for the delayed elution of benzene through the pinhole leak (as determined in control experiments over an inert bed). Thus, the second row represents the average time it takes benzene to elute from an inert bed under the flow conditions used during the catalytic experiment. The bottom three rows list the average benzene elution time from feeds of benzene, *n*-hexane, and 2-methylpentane to the catalyst bed. Due to noise in the response curves, there is some uncertainty in the determination of these average elution times. Thus in addition to a best estimate of the average time, an upper and lower limit is also reported.

The average elution times for the benzene response curves listed in Table 1 may be used as an approximate method to estimate the turnover frequency for benzene production from a given hydrocarbon feed. The average elution time of a benzene peak produced from a hydrocarbon (e.g., *n*-hexane on Pt/KL = 232 ms) consists of the convective gas-phase transport time, the reaction time, and the benzene readsorption/desorption time. The average elution time for benzene in an inert bed (120 ms) is the convective gas-phase transport time of benzene. The difference between these two times (112 ms) is the average reaction time for benzene formation plus the readsorption/desorption time for the benzene formed from *n*-hexane, providing an upper bound on the true reaction time. The inverse on this upper bound average reaction time gives a lower bound on the turnover frequency for benzene production. An upper bound on the turnover frequency may also be estimated. The elution time for a benzene peak from a benzene feed over the catalytic bed (140 ms for Pt/KL) represents convective gas-phase transport time plus the maximum possible time of benzene adsorption/desorption. The difference between the benzene elution time from the *n*-hexane feed and the benzene elution time from the benzene feed (92 ms) leaves the average reaction time minus a quantity due to the overestimation of benzene re-adsorption/desorption from the benzene feed peak (benzene formed by reaction within the bed should have fewer opportunities to re-adsorb than benzene fed directly to the bed). This time provides a lower bound on the average reaction time, and thus the inverse is an upper bound on the turnover frequency.

Table 2 displays benzene turnover frequencies at 425°C for the Pt/Mg(Al)O, Pt/KL, and Pd/Mg(Al)O catalyst, calculated using the above procedure. The uncertainties in the average elution times of benzene response curves exemplified in Table 1 have been considered. The conversion was between 20–30% in all cases, so contributions from reverse reactions should be minor. In addition to upper and lower bounds on the turnover frequency, a best estimate value has also been reported. The calculation of the best estimate turnover frequency assumes that readsorption/desorption of benzene formed from the paraffin feed requires half as much time as adsorption/desorption of benzene from the benzene feed. This is consistent with benzene being produced from the paraffin, on average, midway through the catalyst bed. The equations used for the calculations are summarized below Table 2.

As shown in Table 2, the turnover frequencies for the Pt/KL and the Pt/Mg(Al)O catalyst are similar. Thus, the nature of the support material does not seem to affect the reaction rate significantly. The Pd/Mg(Al)O catalyst, however, has a somewhat lower turnover frequency. The turnover frequencies in Table 2 are generally higher than turnover frequencies previously measured for metal-catalyzed dehydrocyclization reactions (30). This may be explained in several ways. First, in the current calculation only active sites are being considered. In traditional methods of estimating turnover frequencies, the number

TABLE 2

Benzene Turnover Frequencies (sec^{-1}), 425°C

	Pt/Mg(Al)O	Pt/KL	Pd/Mg(Al)O
Mass of catalyst (mg)	6.2	2.5	34
% Conversion[a] *n*-hexane	20	27	21
Benzene turnover frequency, *n*-hexane feed	12(11–13)	9.8(8.6–11)	3.1(2.4–3.7)
Benzene turnover frequency, methylpentane feed	9.6(9.1–10.4)	6.9(6.2–7.5)	2.2(1.8–2.6)

Note. Lower bound benzene turnover frequency, 1/Upper Bound (HC, Cat) − (Bz, Inert); upper bound benzene turnover frequency, 1/Lower Bound (HC, Cat) − Upper Bound (Bz, Cat); best estimate benzene turnover frequency, 1/BestEst (HC, Cat) − Average [(Bz, Inert) + BestEst (Bz, Cat)]. Upper Bound (HC, Cat) = upper bound on average benzene elution time from hydrocarbon feed in catalyst bed. BestEst (Bz, Cat) = best estimate of average benzene elution time from benzene feed in catalyst bed. (Bz, Inert) = average benzene elution time from benzene feed in inert bed.

[a] Based on *n*-hexane conversion to other C_6 products.

TABLE 3

Dependence of Benzene Yield on Carrier Gas, Pt/Mg(Al)O Catalyst, 477°C

Feed Hydrocarbon	H_2 Carrier	He Carrier
n-Hexane	73	8
1-Hexene	93	15
1,5 Hexadiene	100[a]	22

[a] Normalized to a value of 100.

of sites is generally estimated by chemisorption. This may lead to a severe overestimation of the true number of active sites (30). The rate of turnover may also be underestimated in the classical method due to single sites which require an ensemble of exposed metal atoms, or incomplete surface coverage by the reactant. Because the TAP system measures reaction time directly, an estimate of the true rate of turnover which is independent of the number of sites is possible. Finally, because of the small hydrocarbon pulse size in the TAP experiment, the buildup of carbonaceous overlayers on the metal sites is avoided. Thus, the activity of the uncovered metal site itself may be monitored by this technique.

Table 2 also shows the amount of each catalyst that was required to reach 20–30% conversion of *n*-hexane to other C_6 products at 425°C. Because the reactor conditions were virtually identical in all cases this provides a direct measure of the overall activity of the catalyst. The overall activity of a working catalyst is determined by both the speed of reaction on a catalyst site (turnover frequency) and the availability of such sites for reaction.

Table 2 shows that more Pd/Mg(Al)O catalyst was required than Pt/Mg(Al)O catalyst to reach a given conversion level, indicating that the overall activity of the Pd/Mg(Al)O catalyst was lower than that of the Pt/Mg(Al)O catalyst. This is consistent with the results from a previous steady-state reactor study (17). Much less of the Pt/KL catalyst was required than Pt/Mg(Al)O catalyst, indicating that the overall activity of the Pt/KL catalyst is higher (the same trend was also seen at 477°C). The turnover frequency for these two catalysts was similar, which implies that the Pt/KL catalyst has more sites available for *n*-hexane conversion. In contrast, the steady-state reactor results (13, 14) indicated that these two catalysts had similar activity levels on the basis of catalyst mass. The greater activity of the Pt/KL catalyst relative to the Pt/Mg(Al)O catalyst may be masked in the continuous flow reactor. Relatively high hydrocarbon concentrations in the confined space of the zeolite structure may result in steric limitations on transition state formation (10) or surface diffusion, which are more severe in the steady-state reactor than those present under TAP conditions.

The Pt/Mg(Al)O catalyst was examined using both hydrogen and helium as the carrier gas. The effect on the benzene yield of changing the carrier gas is shown in Table 3. Benzene production greatly decreased in the absence of hydrogen flow. Further experiments indicated that other C_6 products were also present, but only in very small quantities. Reproducibility experiments confirmed that this drop in product yield was not due to gradual catalyst deactivation by the hydrocarbon pulses. Thus, it appears that the beneficial effect of gas phase hydrogen in dehydrocyclization is not limited exclusively to preventing coking of the metal sites. Similar behavior has been reported in the literature for reforming catalysts (31–33).

Benzene Selectivities

Previous steady-state experiments at 477°C on these catalysts showed that the Pd/Mg(Al)O catalyst had a higher selectivity for benzene formation than the Pt/Mg(Al)O and Pt/KL catalysts (16). The improved selectivity was not attributed to a decrease in hydrogenolysis reactions, but instead to lower isomer production. A comparison of the selectivities from the TAP system among the major C_6 products formed from *n*-hexane at 477°C and moderate conversions are shown in Table 4. The selectivities reported consider only C_6 components. The

TABLE 4

C_6 Product Selectivities from *n*-Hexane Feed at 477°C

Catalyst	Pt/Mg(Al)O	Pt/KL	Pd/Mg(Al)O	Pt–Re/Al_2O_3	Pt–Re–S/Al_2O_3
% Conversion[a]	23	45	39	23	26
		Product Selectivities			
Hexene	14	18	12	12	10
Methylcyclopentane	10	9	4	16	8
Methylpentane	9	6	1.6	23	12
Benzene	66	67	82	49	69
Forward/reverse[b]	4.2	5.7	17	1.6	4.0

[a] Based on % hexane converted to other C_6 products.
[b] (hexene + benzene)/(methylpentane + methylcyclopentane).

selectivities of the two monofunctional Pt catalysts are closely related. In agreement with the previous steady-state results, the Pd catalyst has a markedly lower tendency to produce methylcyclopentane and methylpentane from the *n*-hexane feed, thus leading to a significantly higher benzene selectivity.

The selectivities among the C_6 products were also determined for the Pt–Re/Al_2O_3 and the Pt–Re/Al_2O_3-fresh catalysts. These results are shown in Table 4. The unsulfided Pt–Re catalyst is less selective than each of the monometallic catalysts shown in Table 4. Sulfiding the catalyst improves the selectivity for benzene production: the coverage of the Re sites with sulfur brings the selectivity of this catalyst in the range of the Pt/Mg(Al)O and Pt/KL catalysts.

CONCLUSIONS

The TAP reactor has been used to study the complex reaction mechanism of C_6 reforming over Pt/Mg(Al)O, Pt/KL, Pd/Mg(Al)O, and Pt–Re/Al_2O_3 (sulfided and unsulfided) catalysts. The unique ability of the TAP system to directly monitor the eluting products from a reacting pulse allowed the reaction mechanism over each catalyst to be determined directly. In all cases the monofunctional reaction pathway on metal, previously reported for the Pt/KL (9) catalyst and Pt supported on nonacidic Al_2O_3 (6), was observed. The Pt/KL and Pt/Mg(Al)O catalysts performed quite similarly from the standpoint of benzene turnover frequency and selectivity. The slow steps in the reaction network involved methylcyclopentane ring opening and 1,6 ring-closure of the linear C_6 molecule, while dehydrogenation steps occurred rapidly. The Pd/Mg(Al)O catalyst showed some fundamental differences in behavior from the Pt catalysts. This catalyst had a lower turnover frequency and higher benzene selectivity than the Pt catalysts. The dehydrogenation steps on this catalyst were significantly slower than on the Pt catalyst.

Under TAP conditions, the reaction network for the Pt–Re/Al_2O_3 catalyst appeared to be the same as for the monofunctional catalysts. Previous investigations of this catalyst (4, 18, 19) showed that the bifunctional mechanism was dominant. This implies the existence of two separate dehydrocyclization pathways on the bifunctional catalyst. Low-pressure conditions such as those used in this study favor the metal-catalyzed dehydrocyclization pathway. However, under high hydrocarbon and hydrogen pressures the number of available metal sites diminishes greatly, thus favoring the bifunctional mechanism.

APPENDIX

Deconvolution of C_6 Component Responses from *m/e* Responses

Table 5 illustrates the problem of overlapping mass signals for potential components of interest. Mass peaks below $m/e = 69$ are not useful for identification of these components, because significant peaks at lower m/e values may also include contributions from smaller (cracked) products.

TABLE 5

QMS Responses for Several C_6 Hydrocarbons

Component	Source	Normalized QMS Responses R_{86}	R_{84}	R_{71}	R_{69}
n-Hexane	1	359		116	
2-Methylpentane	1	148		1000	
3-Methylpentane	1	118		144	
2,2-Dimethylbutane	2	—		1000	
2,3-Dimethylbutane	2	234		1000	
Methylcyclopentane	1		282		1198
Cyclohexane	1		1295		716
1-Hexene	1		409		482
2-Hexene	2		1000		700
3-Hexene[a]	1		581		582
4-Methyl-1-pentene[b]	2		800		1000
Benzene[c]	1	3023			

Note. Source 1, as determined by the QMS from the TAP reactor (71 peak of 2-methylpentane normalized as 1000); source 2, from (34), largest of the two mass response factors normalized to 1000.

[a] *trans* isomer.

[b] One example of numerous branched-C_6 olefin species.

[c] Response for benzene measured at $m/e = 78$.

Consider first the system of C_6 paraffin components, which can be monitored at $m/e = 86$ and $m/e = 71$. Because there are two masses where responses for these components may be measured, two lumps may be constructed. Based on previous studies of reforming reaction networks, it is reasonable to start by leaving *n*-hexane as a single component and forming a lump from the branched-C_6 components. The mass response peaks (expressed as signal intensity as a function of time) may be expressed as

$$I_{86}(t) = m_H(t)R_{86H} + m_B(t)R_{86B} \quad [1]$$

$$I_{71}(t) = m_H(t)R_{71H} + m_B(t)R_{71B}, \quad [2]$$

where subscript H represents *n*-hexane, subscript B represents branched hexanes, $I_j(t)$ = intensity of mass peak j at time t, $m_i(t)$ = moles of component i at time t, and R_{ji} = response factor at mass j for component i.

Simultaneous solution of these two equations yields Eqs. [3] and [4], the true response curves of these pseudo-components in terms of the original mass response curves.

$$m_H(t) = \frac{I_{86}(t) - I_{71}(t)b}{R_{86H}[1 - b/h]} \quad [3]$$

$$m_B(t) = \frac{I_{71}(t)h - I_{86}(t)}{R_{86B}[(h/b) - 1]}, \quad [4]$$

where $h = R_{86H}/R_{71H}$ and $b = R_{86B}/R_{71B}$.

It should be noted that these two equations are also clearly valid for the simpler case where two components have overlapping signals at two masses and no lumping is necessary.

The form of Eqs. [3] and [4] bears closer examination. The denominators of these two expressions contains a group of constants which affects the magnitude of the curves, but not the peak shape. Thus, when looking at normalized versions of these curves, the denominator has no influence. In the numerator, the only constant that appears is the ratio of $m/e = 86$ to $m/e = 71$ for a lumped component. It is also interesting to note that the numerator of the branched-hexane curve (and thus the curve shape) is influenced by the response ratio of *n*-hexane, but not by the response ratio of branched hexanes. Similarly, the numerator of the response curve for *n*-hexane includes only the response ratio of branched hexanes.

For a case where the QMS responses for the lumped components are similar, Eqs. [3] and [4] would be sufficient to deconvolute the pseudocomponent response curves. However, Table 5 indicates that, in the case of the branched hexanes, the QMS responses of the four lumped components are significantly different. This makes it impossible to determine the appropriate values for R_{86B} and R_{71B} without further information about the concentrations of the components in the branched-hexane lump. Two assumptions permit the evaluation of the necessary parameters for this lump. The first assumption is that the quantity of dimethylbutanes is small relative to methylpentanes. This is usually the case in reforming (1), and was found in the previous experiments on the monofunctional catalysts utilized in this study (17). The second assumption is that the ratio of 2-methylpentane to 3-methylpentane in the lump is 2 : 1. In the main text evidence is given that the formation of methylpentanes from linear C_6 proceeds through a C_5 cyclic intermediate. The 2 : 1 value for the 2-methylpentane : 3-methylpentane ratio assumes purely statistical ring hydrogenolysis of methylcyclopentane, and has been previously reported for monofunctional reforming catalysts (6, 9, 29). Using the first assumption allows Eqs. 1 and 2 to be rewritten as

$$I_{86}(t) = m_H(t)R_{86H} + m_{2P}(t)R_{86-2P} + m_{3P}(t)R_{86-3P} \quad [5]$$

$$I_{71}(t) = m_H(t)R_{71H} + m_{2P}(t)R_{71-2P} + m_{3P}(t)R_{71-3P}, \quad [6]$$

where $m_{kP}(t)$ = moles of *k*-methylpentane at time *t* and R_{j-kP} = response factor at mass *j* for *k*-methylpentane.

Applying the second assumption regarding the ratio of the methylpentanes leads to Eqs. [7] and [8]:

$$m_{2P}(t) = \frac{2}{3}m_B(t) \quad [7]$$

$$m_{3P}(t) = \frac{1}{3}m_B(t). \quad [8]$$

Substitution of Eqs. [7] and [8] into Eqs. [5] and [6] yields Eqs. [9] and [10]:

$$I_{86}(t) = m_H(t)R_{86H} + m_B(t)\left[\frac{2}{3}R_{86\text{-}2P} + \frac{1}{3}R_{86\text{-}3P}\right] \quad [9]$$

$$I_{71}(t) = m_H(t)R_{71H} + m_B(t)\left[\frac{2}{3}R_{71\text{-}2P} + \frac{1}{3}R_{71\text{-}3P}\right]. \quad [10]$$

Comparison of Eqs. [9] and [10] with Eqs. [1] and [2] shows that Eqs. [11] and [12] may be used to evaluate R_{86B} and R_{71B} in terms of the values for 2-methylpentane and 3-methylpentane from Table 5.

$$R_{86B} = \frac{R_{86-3P} + 2R_{86-2P}}{3} \quad [11]$$

$$R_{71B} = \frac{R_{71-3P} + 2R_{71-2P}}{3}. \quad [12]$$

Application of these equations leads to values of $R_{86B} = 138$ and $R_{71B} = 716$.

A similar derivation may be performed to deconvolute the responses of methylcyclopentane, normal hexenes, branched hexenes, and cyclohexane curves at $m/e = 69$ and $m/e = 84$. This case appears to be more difficult, because there are now more components to consider. It is beneficial to leave methylcyclopentane as a single component and to put all of the other components into a lump. A pair of equations parallel to [3] and [4] may be derived

$$m_J(t) = \frac{I_{84}(t) - I_{69}(t)q}{R_{84Q}\left[1 - \frac{q}{j}\right]} \quad [13]$$

$$m_Q(t) = \frac{I_{69}(t)j - I_{84}(t)}{R_{84Q}\left[\frac{j}{q} - 1\right]}, \quad [14]$$

where subscript J represents branched hexenes, *n*-hexenes, and cyclohexane, subscript Q represents methylcyclopentane, $j = R_{84J}/R_{69J}$, and $q = R_{84Q}/R_{69Q}$.

The problem of estimating R_{84J} and R_{69J} now persists, because of the different response factors from the numerous species in this lump. Careful consideration of the resulting m_J peak in the reaction network (which may be determined using the numerator of Eq. [13] and thus requires only the parameter *q* from pure methylcyclopen-

tane) allowed further conclusions about the identity of the components represented by this peak. In general, the peak position indicated that branched hexenes were not significantly contributing to the peak shape, thus implying that they could be removed from the lump. For reasons discussed in the main text, the hexene contribution was generally assumed to be much greater than the cyclohexane contribution. As indicated in Table 5, the normal hexenes all have similar response factors, so simply averaging their responses at $m/e = 84$ and $m/e = 69$ should allow a reasonable estimate for the parameters R_{84J} and R_{69J}. Averaging the calibrated responses for 1-hexene and 3-hexene shown in Table 5 gives values of $R_{84J} = 495$ and $R_{69J} = 530$. Equations [13] and [14] can then be applied directly.

ACKNOWLEDGMENTS

Discussions with Glenn Creten, Marie-Francoise Reyniers, and Jan Verstraete, and the financial support of FKFO and the Center of Excellence Award of The Ministerie voor de Programmatie van Het Wetenschapsbeleid are gratefully acknowledged.

REFERENCES

1. Sinfelt, J. H., *Catal. Rev. Sci. Tech.* **1,** 257 (1981).
2. Menon, P. G., and Prasad, J., *in* "Proceedings 6th International Congress on Catalysis, London, 1976)" (G. C. Bond, P. B. Wells, and F. C. Tompkins, Eds.), p. 1061. The Chemical Society, London, 1977.
3. Marin, G. B., and Froment, G. F., *Chem. Eng. Sci.* **37,** 759 (1982).
4. Van Trimpont, P. A., Marin, G. B., and Froment, G. F., *Appl. Catal.* **17,** 161, (1985).
5. Davis, B. H., and Venuto, P. B., *J. Catal.* **15,** 363 (1969).
6. Dautzenberg, F. M., and Platteeuw, J. C., *J. Catal.* **19,** 41 (1970).
7. Gault, F. G., *Adv. Catal.* **30,** 1 (1981).
8. Bernard, J. R., *in* "Proceedings, 5th International Zeolite Conference" (L. V. Rees, Ed.), p. 686. Heyden, London, 1980.
9. Lane, G. S., Modica, F. S., and Miller, J. T., *J. Catal.* **129,** 145 (1991).
10. Derouane, E. G., and Vanderveken, D. J., *Appl. Catal.* **54,** L15 (1988).
11. Derouane, E. G., Andre, J. M., and Lucas, A. A., *J. Catal.* **110,** 58 (1988).
12. Tamm, P. W., Mohr, D. H., and Wilson, C. R., *Stud. Surf. Sci. Catal.* **38,** 335 (1988).
13. Davis, R. J., and Derouane, E. G., *J. Catal.* **132,** 269 (1991).
14. Davis, R. J., and Derouane, E. G., *Nature* **349,** 313 (1991).
15. Schaper, H., Berg-Slot, J. J., and Stork, W. H. J., *Appl. Catal.* **54,** 79 (1989).
16. Derouane, E. G., Jullien-Lardot, V., Pasau-Claerbout, A., Blom, N. J., and Nielsen, P. E. H., *in* "Proceedings, 10th International Congress on Catalysis, Budapest, 1992" (L. Guczi, F. Solymosi, and P. Tetenyi, Eds.) p. 1031. Akadémiai Kiadó, Budapest, 1993.
17. Derouane, E. G., unpublished data, 1992.
18. Van Trimpont, P. A., Marin, G. B., and Froment, G. F., *Ind. Eng. Chem. Fundam.* **25,** 544 (1986).
19. Van Trimpont, P. A., Marin, G. B., and Froment, G. F., *Appl. Catal.* **24,** 53 (1986).
20. Van Trimpont, P. A., Ph.D. dissertation, University of Gent, 1984.
21. Gleaves, J. T., Ebner, J. R., and Kuechler, T. C., *Catal. Rev.—Sci. Eng.* **25,** 1 (1989).
22. Coulson, D. R., Mills, P. L., Kourtakis, K., Lerou, J. J., and Manzer, L. E., *Stud. Surf. Sci. Catal.* **72,** 305 (1992).
23. Amir-Ebrahimi, V., and Gault, F. G., *J. Chem. Soc., Faraday Trans 1* **76,** 1735 (1980).
24. Barron, Y., Cornet, D., Maire, G., and Gault, F. G., *J. Catal.* **2,** 152 (1963).
25. Barron, Y., Maire, G., Muller, J. M., and Gault, F. G., *J. Catal.* **5,** 428 (1966).
26. Van Trimpont, P. A., Marin, G. B., and Froment, G. F., *Ind. Eng. Chem. Res.* **27,** 51 (1988).
27. Nix, P. S., and Weisz, P. B., *J. Catal.* **3,** 179 (1964).
28. Shum, V. K., Butt, J. B., and Sachtler, W. M. H., *Appl. Catal.* **11,** 151 (1984).
29. Sivasanker, S., and Padalkar, S. R., *Appl. Catal.* **39,** 123 (1988).
30. Somorjai, G. A., *in* "Catalyst Design, Progress and Perspectives" (L. L. Hegedus, Ed.), p. 11. Wiley, New York, 1987.
31. Zimmer, H., Dobrovolszky, M., Tetenyi, P., and Pall, Z., *J. Phys. Chem.* **90,** 4758 (1986).
32. Paal, Z., *in* "Hydrogen Effects in Catalysis" (Z. Pall and P. G. Menon, Eds), p. 449. Dekker, New York, 1988.
33. Paal, Z., Groeneweg, H., and Pall-Lukacs, J., *J. Chem. Soc., Faraday Trans.* **86,** 3159 (1990).
34. Cornu, A., and Massot, R., "Compilation of Mass Spectral Data." Heydon & Son, London, 1966.